

Hyporheic Exchange in the Petit Buëch, Southern France

MSc thesis
Timmy Grimberg
Utrecht University, 2013

Supervised by: Dr. Marcel van der Perk

Abstract

A point bar along the Petit Buëch in southern France was studied for the effect of the interaction between groundwater and surface water. This so-called hyporheic exchange was clearly visible at multiple locations on the point bar. Residence time increases when water from the river infiltrates into the subsurface, influencing the transportation of nutrients and pollutants. A fieldwork was performed to do measurements on elevation, porosity and hydraulic conductivity. Grain size measurements were performed to calculate a porosity of 0.18 to 0.35. Hydraulic conductivity was calculated using porosity and groundwater velocity, resulting in an average hydraulic conductivity of 0.16 m/s. In ArcGIS the measurements were interpolated. Interpolations showed locations of large hydraulic conductivity in the inland part of the study area. In groundwater flow model MODFLOW, random fields of hydraulic conductivity were imported for particle tracing experiments in PMPATH. These resulted in residence time distributions having an average residence time of ~ 20 days. Fluxes were calculated along the river boundary, indicating a surplus of water infiltrating into the area of 1.6 m/s. Either the water exfiltrates into gullies on the point bar or elsewhere beyond the study area.

Table of Contents

1. Introduction	5
2. Methods and Materials	9
2.1 Area / site description	9
2.2 Mapping the area	9
2.3 Measuring hydraulic conductivity	11
<i>Groundwater flow velocity</i>	11
<i>Hydraulic gradient</i>	12
<i>Porosity measurements</i>	12
<i>Hydraulic Conductivity</i>	13
2.4 Modelling the data (MODFLOW)	14
3. Results and Discussion	17
3.1 Morphological units	17
3.2 Hydraulic Conductivity	19
3.3 MODFLOW model	24
<i>Model input</i>	24
<i>Field Generator and correlation length</i>	25
<i>Infiltration and exfiltration fluxes</i>	27
<i>Simulation A</i>	29
<i>Simulation B</i>	31
3.4 Recommendations	32
4. Conclusions	33
5. Acknowledgements	34
6. References	35

1. Introduction

Rivers are of utmost importance for humanity while covering only 0.0002 percent of the total amount of water in the world (Gleick, 1996). Besides being one of the main sources for drinking water and food, rivers are used for transportation, as source for hydropower and as a defensive measure.

Exploitation of rivers for waste disposal might be of major influence downstream. Flora, fauna and humans are all dependant on rivers, therefore much research is performed on hydrological processes in rivers. Contaminants might flow downstream ending and dispersing into the ocean. However, a small percentage of pollutants might infiltrate into the subsurface and influence hydrological processes. Therefore it is important to know what will happen to pollutants in the river.

The transport of nutrients and pollutants in rivers is an important issue for the management of rivers. Hydrological processes in rivers influence the behaviour of those substances and therefore they are important for the ecology. For instance, pollution in the subsurface can be a major issue for ecology, because the subsurface is a source for irrigation, crop cultivation and nature areas (Merkx, 2011).

Several important hydrological processes take place in the transition zone between rivers and aquifers. In this zone, the hyporheic zone, hydrological processes include river metabolism, distribution of microfauna and heat transport (Cardenas, 2009). Exchange from surface water to groundwater may cause the residence time of pollutants and nutrients to increase. This enlarges environmental and ecological risks. Processes affecting the interaction between surface and subsurface water have to be studied to understand the transport of pollutants. A study was performed on a river floodplain in France to evaluate these processes. At various locations in the study area, groundwater exfiltrates towards the surface, indicating locations of interaction between surface water and groundwater.

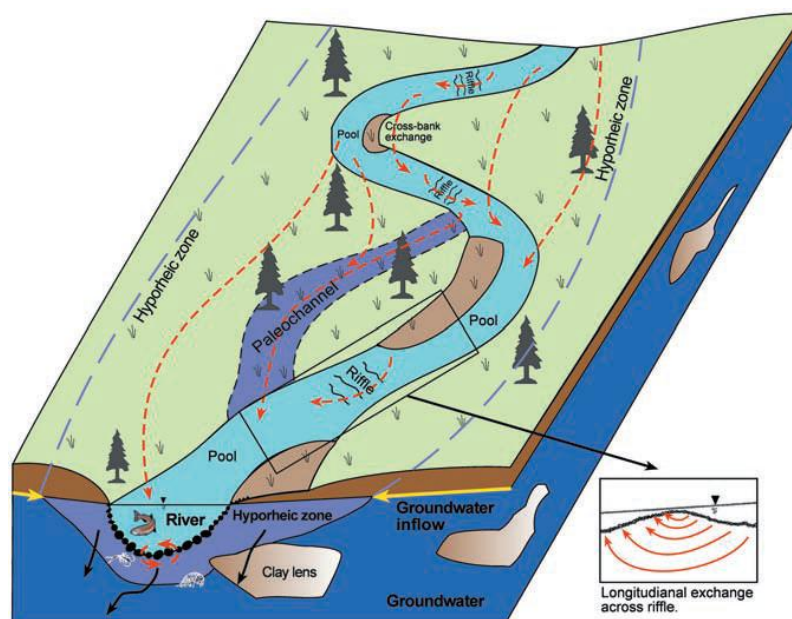


Figure 1 – Overview of the hyporheic zone (Torina and Buffington, 2009). Red flow paths represent hyporheic flow.

The hyporheic zone can be defined as the interface between surface and groundwater in near-stream sediments (Lautz and Siegel, 2006). Broader definitions are given by Cardenas et al. (2004), defining the hyporheic zone as the area where water infiltrates from streams, flows through streambed sediments and stream banks, and returns to the surface after relatively short pathways. An overview of hyporheic flow in a meandering river is given in Figure 1.

The exchange of surface and subsurface water has already been studied carefully during the last decades. Interaction between the surface flow and topographical features within the streambed cause water to flow in and out of the hyporheic zone. Hyporheic exchange may cause nutrients and pollutants to reach the hyporheic zone. This process causes changes in the growth of microorganisms and biotic processes (Boano et al., 2007-2).

Examples of organisms abundant in surface waters are periphytons and macrophytes. These organisms can live in surface waters due to its high oxygen levels caused by direct contact with the atmosphere. Nutrients entering the hyporheic zone can cause the surface waters to become anaerobic due to microbial processes (Dent and Henry, 1999). The change in oxygen level has radical consequences for the amount of organisms.

The hyporheic zone, in which water velocity is lower than in the main stream, is called transient storage zone (Stofleth et al., 2007). Research has been performed on transient storage zones: interaction between the hyporheic zone and the underlying aquifer. This includes a study of Boano et al. (2007-2), who used models to demonstrate that water exchange flux and residence times are influenced by changes in river discharge. Other studies show how transport of chemicals is influenced by groundwater, using tracer injections (Marion et al., 2008), and modelling hyporheic exchange at smaller scales (e.g. ripples) (Boano et al., 2007-1).

A different factor that increases the influence of pollutants on the hyporheic zone is caused by retention during the interaction between river and hyporheic zone. That leads to stagnant zones of water such as pools, side channels and wetland areas. These stagnant water zones have their own zones where groundwater and surface water mix apart from the river – groundwater interaction zones (De Smedt, 2007 and Marion et al., 2008). In breakthrough curves the slow release from these zones is recognizable as a long tail (Ge and Boufadel, 2006). The residence time is increased by these processes, where flow paths caused by stream flow velocity show the shortest residence time and hyporheic exchanged causes the longest residence time (Gooseff et al., 2003).

Several processes cause hyporheic exchange in the streambed of a channel. One of those processes is the change of pressure within the hyporheic zone (Figure 2, upper picture). In turbulent rivers, obstructions on streambed topography cause high pressure on the upstream side and low pressure downstream. At the upstream side water enters the bed, leaving at the downstream side (Worman et al., 2002).

Another factor causing hyporheic exchange is the composition of the sediment (Figure 2, lower picture). Groundwater flowing through the sediment depends on the hydraulic conductivity of the sediment. Impervious layers cause reduction in volume of usable sediments for groundwater flow, and therefore the flow path is altered (Storey et al., 2003 and Tonina and Buffington, 2009).

On point bars of meandering rivers, hyporheic exchange can be caused by changes in hydraulic head. Topography differences may cause the hydraulic head to be above the topography level, therefore groundwater will discharge into swales due to exfiltration. Subsurface flow changes to surface flow, forming shortcuts on the point bar.

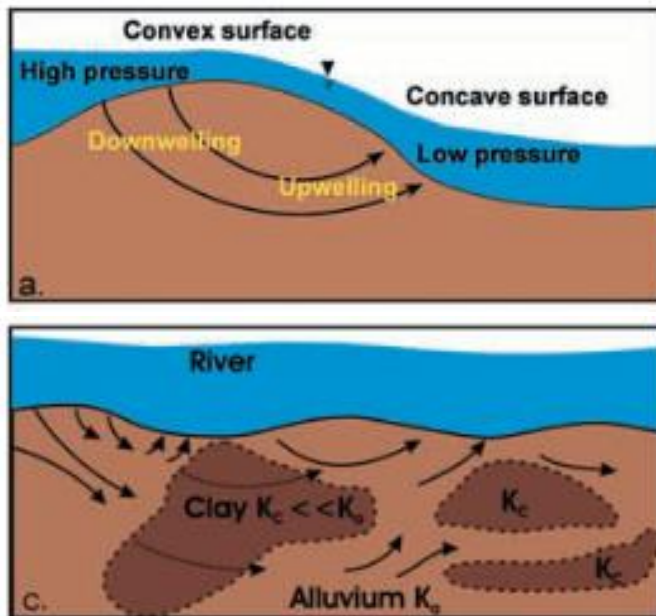


Figure 2 – Mechanics of hyporheic exchange in the riverbed: change of pressure (upper picture) and change of hydraulic conductivity (lower picture) (Tonina and Buffington, 2009)

Several approaches exist to describe the process of hyporheic exchange. Pressure gradients over the stream channel boundary cause hyporheic exchange along morphological features like meanders, bars and bed forms (Stonedahl et al., 2010 and Worman et al., 2007). Some studies focus on small scale features like bed forms (Cardenas et al., 2004) while some focus on larger scale features like stream meanders (Boano et al., 2007) or multiscale features (Stonedahl et al., 2010). A popular approach for modelling is the usage of stream solute advection dispersion models (Gooseff et al., 2003). These models assume exponential residence time distribution (RTD) of water in bank storage (Harvey and Bencala, 1993). One of the most recent approaches is RTD modelling, where RTD's are fitted to observed data (Haggerty et al., 2002).

Hyporheic exchange can be measured using several methods, e.g. hydrometric instrumentation, tracer tests, discharge measurements and water temperature measurements. Hydrometric instrumentation includes the usage of bail and slug tests to measure the hydraulic conductivity. Using these tests, the water level in the well is increased (slug test) or decreased (bail test) (Rayne et al., 1996). The data from both tests can be used to calculate the hydraulic conductivity by a model of Bouwer and Rice (1976). According to Cey et al. (1998), hyporheic exchange is mainly dependant on hydraulic conductivity. However hydraulic conductivity is difficult to measure in highly heterogeneous soils because of the presence of layers with low conductivity.

The aim of this study is to better understand the process of hyporheic exchange in the study area by using hydrological models. The amount of hyporheic groundwater flow through the point bar system is quantified as well as the residence time distributions of groundwater in the point bar. A fieldwork area was defined based on the visibility and accessibility of the hyporheic zone. Consequently, a model was developed to describe the hyporheic exchange. It may be possible to draw conclusions on comparable or larger areas by extrapolating the results.

All methods that are used to develop the hydrological model are described in the Methods section. These methods include field sampling techniques. The results of the measurements and the models based on these measurements are given in the Results Section. At the end of the Results Section, the models were used to create residence time distributions.

2. Methods and Materials

2.1 Area / site description

The point bar of a meandering mountain river in France was used for the research on hyporheic exchange. The river Le Petit Buëch in Southern France (Hautes Alpes department) is a typical whitewater river which carries many rocks and boulders, especially during melting season. A characteristic of whitewater rivers is that during melting season the discharge of the river becomes larger and erosion broadens the river.

The source of the river lies within the Pré Alpes du Sud, near the small village of Chaudun, north of Gap. Flowing generally from northeast to southwest, Le Petit Buëch merges with its main tributary Le Béoux near Veynes. Further downstream, the river merges with Le Grand Buëch into Le Buëch near Serres. Experiments performed during previous fieldwork showed a maximum flow velocity of 0.6 to 0.7 m/s.

The fieldwork area was defined as a point bar of one of the meanders near the village of La Bâtie-Montsaléon (

Figure 3). Along this point bar, the river flows from east to west. At several locations, including the research area, the river was broadened by tens of meters due to bank erosion during the last decades. One effect of the enlarged discharge during the melting season is that the course of the river changes and therefore the morphological patterns change as well. At some locations on the point bar, remnants of the former river course remain visible in the form of swales and ridges, while the course of the main channel changes. At other locations, pools of stagnant water remain visible on the point bar.

To develop a hydrological model for the research area, the entire area was mapped and different morphological units were distinguished. Rough sketches were made from visible observations and more detailed maps were made using aerial photographs. The aerial photographs were made during the fieldwork using a miniature helicopter. Using aerial photographs of the current situation prevented working with former morphological features while modelling. In ArcGIS, all aerial photographs were filtered and assembled to make one compilation. The aerial photograph was orthorectified using GPS measurements from recognizable points in the area.

2.2 Mapping the area

Differential GPS (DGPS) measurements were performed across the fieldwork area to create a height model using ArcGIS. DGPS improves the accuracy of normal GPS measurements by using a local reference station with known GPS coordinates.¹ In this study the local reference station was placed on an elevated location near the edge of the river. The entire fieldwork area could be viewed

¹ For a detailed description of the advantage of using DGPS over GPS, the Trimble tutorial is recommended: http://ww2.trimble.com/gps_tutorial/sub_adv.aspx

from this reference station and therefore precise DGPS measurements were made.

The larger the number of DGPS measurements across the fieldwork area is, the more precise the Digital Elevation Model (DEM) could be. DGPS measurements were performed on random locations and on locations with differentiating morphological features such as small ridges. Many small gullies and swales in the area close to the river showed small differences in height and therefore also these locations were measured. Besides those morphological features, some transects were made perpendicular to the river and through the former river courses and swales. These transects were used in order to have a better overview of the research area.

Different interpolation methods can be used for the DGPS measurements in ArcGIS. The most used interpolation methods in ArcGIS include Inverse Distance Weighted (IDW) interpolation, kriging and Topo to Raster. IDW uses average values of the sample data in the neighbourhood of each cell. Kriging generates an estimated surface from a scattered set of points using a semivariogram which represents the spatial correlation structure. Finally, the Topo to Raster method creates a surface representing a natural drainage surface and preserving ridgelines and stream networks (based on ANUDEM by Hutchinson 1988, 1989). All of these interpolation methods were tested using different settings. No statistical analyses were performed on the inter-polations, however the method that most corresponded to the visually observed morphology was chosen. In this study, the Topo to Raster method was chosen for further usage. From the Digital Elevation Model a raster map was created with a cell size of 1 meter. The raster map had an extension corresponding to the size of the research area on the rectified aerial photograph.

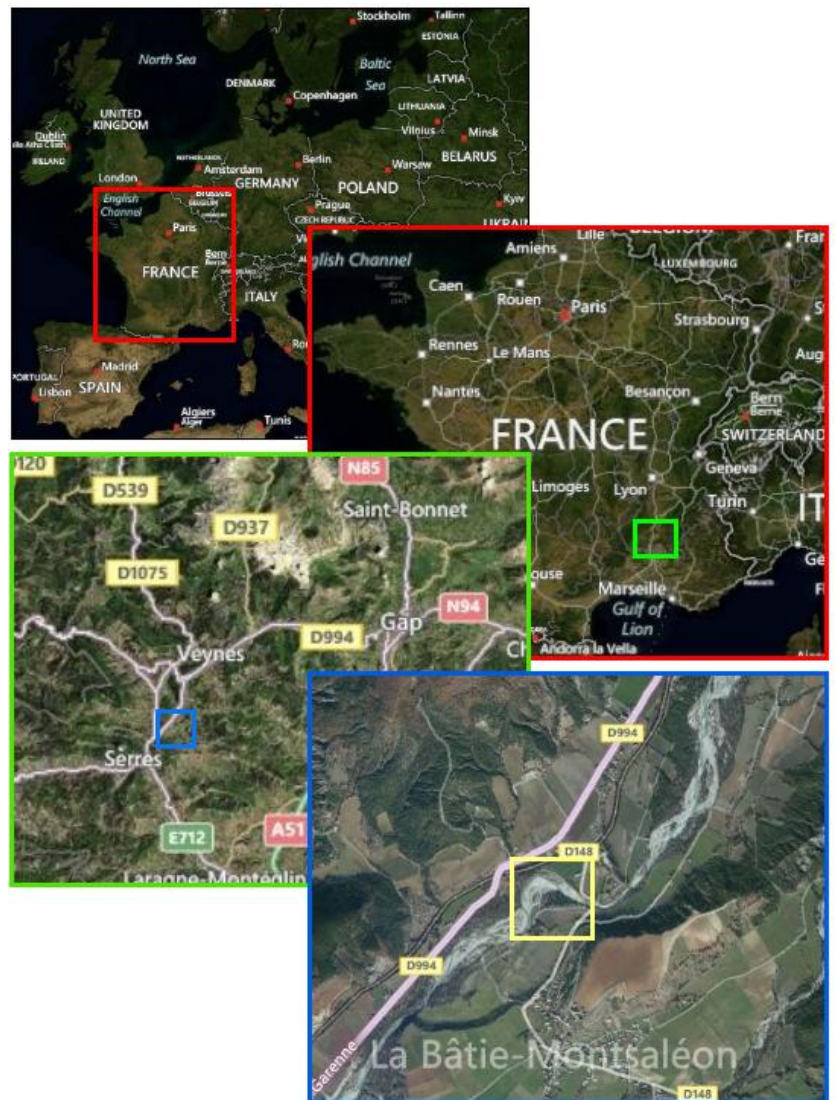


Figure 3 – Overview of the research area (yellow square)
(Adapted from Bingmaps)

2.3 Measuring hydraulic conductivity

Measurements were performed in order to calculate the hydraulic conductivity (K) to research the hyporheic exchange on the point bar of the river. The K -value can be calculated using a form of Darcy's Law:

$$K = \frac{q}{i} \quad (1)$$

in which K is the hydraulic conductivity (m/s), q is Darcy velocity (m/s) and i is the hydraulic gradient (dh/dx). Darcy velocity is defined by groundwater flow velocity divided by the porosity. From porosity measurements, interpolations were used in the calculations.

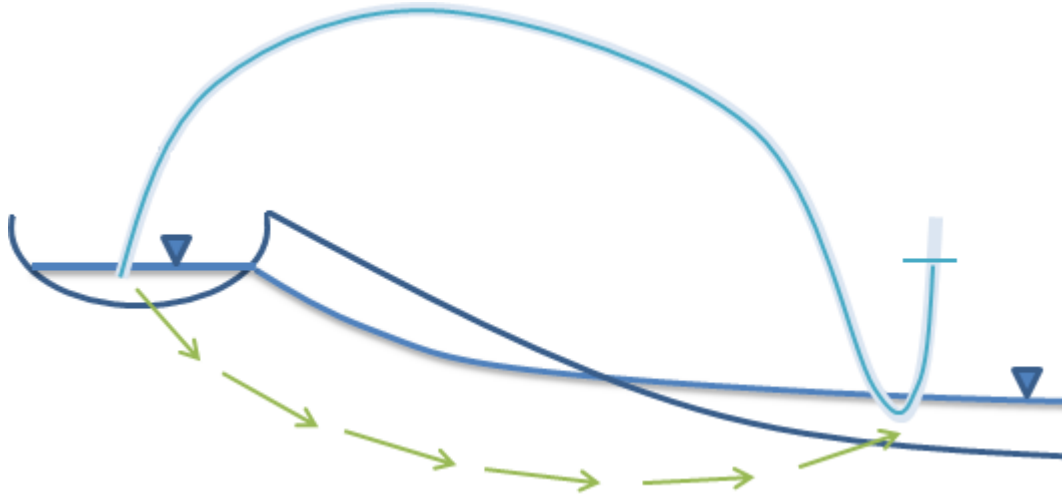


Figure 4 – Sketch of the experiments performed for measuring the hydraulic conductivity. Dark blue line represents the water level. Green arrows represent uranine flow. At the point of exfiltration EC measurements were performed. Light blue line represents tube filled with water. The difference of water level within the tube with the surface water is used for the hydraulic gradient.

Groundwater flow velocity

Measurements on groundwater flow velocity were performed on locations where groundwater exfiltrates and discharges into gullies, and on locations where water from the sediments visibly flows out into the main channel. On places with visible exfiltration, the flow direction of groundwater in the neighbouring area would be towards that location. At 39 locations in the research area near the main channel or swales, tracer experiments were performed. A hole was dug down to the groundwater level (Figure 4). Uranine dye tracer was poured into the hole to locate the exact point of exfiltration of groundwater flowing through the hole. Uranine is a red synthetic organic compound which is highly soluble in water and alcohol. Dissolving uranine in water creates a highly fluorescent solution. After pouring the uranine solution into the hole, the fluorescence appears at location of exfiltration (green arrows in Figure 4). This is an indication of the direction of groundwater flow.

Electrical conductivity (EC) measurements were performed after the location of exfiltration was known to create breakthrough curves. A strong salt solution was made by dissolving approximately 250 grams of salt in 1 litre of water. Addition of salt to water increases the EC, which can be measured using an EC-meter. The electrode of the EC-meter was placed into the water on the location of exfiltration. After that, the entire salt solution was released instantaneously into the hole. From the moment that the salt solution was added to the groundwater

until the EC returned to its initial value the EC of the exfiltrating water was monitored every ten seconds. All monitored EC-values visualized in a graph results in a breakthrough curve.

Breakthrough curves are used for the calculation of groundwater flow velocity. Either the time measured until the maximum EC (t_{max}) or the time measured until 50% of the area beneath the curve (t_{50}) can be used as time to breakthrough. For this research, the latter was chosen representing the time until 50% of the salt tracer has passed the measurement point. Besides the tracer experiments, the distance between the hole and the point of exfiltration was measured, together with the flow direction of both points.

Hydraulic gradient

The calculation of hydraulic conductivity requires the hydraulic gradient, being the gradient between two hydraulic heads over the length of the flow path. The hydraulic head was measured at both the location of the hole and the point of exfiltration. Both DGPS and GPS were not precisely enough to measure the difference in hydraulic head and therefore a method based on communicating vessels was used. A transparent tube was entirely filled with water and one end of the tube was put into the groundwater of the hole. The other side of the tube had reached water level equal to the groundwater level of the hole after reaching equilibrium (Figure 4). The difference in height between the water level in the tube and the surface water on the exfiltration point was measured. Dividing that difference of hydraulic head by the distance between the hole and the exfiltration point gave the hydraulic gradient.

Porosity measurements

The porosity of the soil was needed for the formation of a hydrological model. Therefore, sieve experiments were performed across the fieldwork area. As the area was divided into different morphological units, several locations for sieve experiments were chosen. The distribution of the grain sizes at the location was calculated for these experiments. The gravel was sundried to loosen all particles from each other. After that, the gravel sample was placed on the sieve with the largest mesh-size and the residue was weighed. This procedure was continued to smaller mesh-sizes. The cumulative weight percentages of the weighed residues were plotted on semi-log scales to obtain the size distribution for each sample.

Estimations of the porosity at the sample locations were made from the grain size distribution, using the following equations based on data from Frings et al. (2008) and Beard and Weyl (1973):

$$n = 0.435 - 0.122\sigma \text{ for } \sigma \leq 1.0 \quad \text{and} \quad n = 0.341 - 0.028\sigma \text{ for } \sigma > 1.0 \quad (2)$$

with

$$\sigma = \frac{\left(\frac{\ln \varphi_{84}}{\ln 2}\right) - \left(\frac{\ln \varphi_{16}}{\ln 2}\right)}{4}$$

where n is porosity and φ_{84} and φ_{16} are the grain sizes at which respectively 84 and 16 percent of the sediment is finer than the specified diameter. The values for φ_{84} and φ_{16} were obtained using the grain size distributions. For the exact values, logarithmic interpolation was performed.

Interpolation of the porosity measurements was needed to plot the porosity for the entire area, because only 13 measurements were performed. From these locations, the porosity values were plotted in ArcGIS. As stated above for the interpolation of DGPS values, ArcGIS has different interpolation methods which could be used. The method to interpolate the porosity measurements was chosen based on experimentation and best fit. For the interpolation of porosity, the Topo to Raster method was used.

Hydraulic Conductivity

Darcy velocity was calculated on 39 locations using the interpolated porosity and the exact groundwater flow velocity. The hydraulic conductivity was calculated on these locations using Darcy's Law (Equation 1). From all these locations the coordinates were known and therefore they could be plotted in an ArcGIS map. As with the porosity measurements, preferably there should have been measurements at all locations across the study area. An interpolation was made for the entire area due to the limited number of measurements. The Topo to Raster method of ArcGIS was used for interpolation to be consistent with other non-topographical interpolations. The interpolation was exported to an ASCII-file to import the data into hydrological modelling program PMWIN and its particle tracing model PMPATH.

An analysis of variance (ANOVA) between the interpolation and the morphological units was performed to analyse the interpolation of the hydraulic conductivity statistically. The morphological units were determined independent from the interpolations and therefore it was possible to perform ANOVA on the hydraulic conductivity. For the ANOVA 1000 locations in the study area were randomly chosen using ArcGIS. Together with the hydraulic conductivity, the representing morphological unit was assigned to every location, with 1 being least vegetated and 5 being most vegetated. Note that morphological unit number 6 (with most vegetation) was left out of the analysis due to its small size and small number of locations. ANOVA was performed over log transformed values. Additional analysis was performed on the differences between the morphological units.

Unlike the measurements for the creation of a Digital Elevation Model, the locations for the experiments regarding hydraulic conductivity were measured using a handheld GPS. These coordinates were corrected in ArcGIS for a deviation caused by the device. The correction was performed according to their location based on the orthorectified aerial photograph.

2.4 Modelling the data (MODFLOW)

The collected data which were needed for creating a hydrological model were imported into the MODFLOW model. MODFLOW is a three dimensional groundwater flow model and requires multiple parameters to be imported. As pre- and post-processor the program Processing MODFLOW for Windows (PMWIN) was used. Particle tracking program PMPATH is included in the PMWIN package. Flow lines and flow paths can be simulated using PMPATH.

In PMWIN, the following parameters and initial conditions were specified before running the model:

- Mesh size and layer property (model extension)
- Cell status
- Time parameters
- Initial hydraulic head
- Vertical and horizontal hydraulic conductivity
- Effective porosity

The model extension was chosen based on the Digital Elevation Model (DEM) created in ArcGIS. That results in a grid size and cell size which is exchangeable between the ArcGIS model and the MODFLOW model. More details and longer processing times would be needed when using a smaller cell size. If the cell size would be too large, multiple measurements could be located in one cell. Therefore a medium size of cells was chosen by using cells of 1 square meter. That resulted in a grid with an extension of 322 by 239 meters. Details of hyporheic exchange would be visible in cells of 1 square meter, as was confirmed by field observations.

Also the thickness and the number of layers of the MODFLOW model were specified in the model extension. The model was tested by using different thickness of layers. The thickness of the layers was chosen by testing its influence on the residence time of particles. Three particles were released using particle tracing program PMPATH to show the relation between layer thickness and residence time. For these tests, an average hydraulic conductivity was chosen for the entire grid. Further methods were dependent on the results of these tests. The number of layers was chosen to be in accordance with the differences in topographical elevation. The layers had to be specified whether they were confined or unconfined layers, based on the nature of the area and their transmissivity. The transmissivity is set to be calculated by the MODFLOW model by using the horizontal hydraulic conductivity and the elevations for the top and bottom of the layers (Chiang, 2005). These were specified by importing ASCII files containing the DGPS interpolations created using ArcGIS. The elevation of the lower lying layers was specified by the layer thickness.

The cell status was assigned using the IBOUND functionality of PMWIN. Not all cells within the 322 by 239 grid were used for the hydrological model due to the particular shape of the research area. Using IBOUND it was specified whether cells represent constant head cells (i.e. cells representing the river at the boundary of the model area, value -1), inactive cells (i.e. cells outside the model area, value 0) or active cells (i.e. cells within the model area, value 1). A map indicating the outline of the research area was imported into the MODFLOW model and used to represent the model boundaries. This map was extracted from the aerial photograph of the study area.

The time parameters were defined to calculate the model in steady state. Steady state was chosen because the particle tracing program PMPATH does not need transient flow types for the formation of residence time curves. Using transient flow types would disrupt the process of being able to compare different simulations as flow changes through time.

Next, the initial hydraulic head was specified. The initial hydraulic head is used as starting value for the iterative equation solvers of MODFLOW. Therefore, the constant head boundaries should have an input value, while the others are calculated by MODFLOW.

ASCII files were created using the Raster to ASCII functionality in ArcGIS to import the interpolated values for horizontal hydraulic conductivity and effective porosity. Because of using multiple layers, there is a certain vertical conductance (leakance) between the layers (Chiang and Kinzelbach, 1998). This leakance was set to be calculated by the model and therefore the vertical hydraulic conductivity will not be specified.

The particle tracking functionality of PMPATH, which is part of the PMWIN package, was used for creating residence time distributions in the study area. In PMPATH, particles were added on multiple locations across the study area along the northern boundary. The locations were chosen depending on the flow of groundwater through the area. Particles added along the northern boundary of the study area would flow through the point bar to the western and southern boundary, due to the flow direction of the river.

The MODFLOW model was run using the values for the interpolated horizontal hydraulic conductivity to get the residence times for the situation in the field. Grids of randomly generated horizontal hydraulic conductivities were used in the formation of residence time distributions. The randomly generated hydraulic conductivity grids were generated using the Field Generator, which is included in the PMWIN package. The random fields generated by the Field Generator were based on the average hydraulic conductivity, the standard deviation of the hydraulic conductivity and the correlation between the values. For the correlation, the ratios between correlation length and field width along rows and columns were needed.

Two methods were used to estimate the correlation between neighbouring cells regarding hydraulic conductivity. The first method is the usage of the correlation function in Microsoft Excel. The correlation function in Excel uses the correlation between two log transformed values of hydraulic conductivity. The correlation was plotted against the associated distance between the two values. To

determine the correlation length, the distance should be in accordance to the cell size of the model.

The second method is the formation of a semivariogram using the module for Geostatistical modelling (Gstat) of PCRaster (Pebesma, 2001). This method fits a semivariogram to the measured data in case they show a spatial relationship. From the semivariogram, the correlation length and the semivariance can be extracted.

The randomly generated hydraulic conductivity fields were imported into Excel to verify their values. Their average values and standard deviations were calculated. These were compared to the average value of the interpolated hydraulic conductivities and its standard deviation. The difference between the randomly generated fields and the interpolated field is an indication of the reliability of the results of the Field Generator.

Two simulations were performed using the randomly generated grids to visualize groundwater flow paths through the study area. These simulations were imported to PMPATH, in which particles were released and traced during their residence in the area. In Simulation A, 50 MODFLOW simulations were performed for the formation of residence time distributions on six locations. These locations were chosen along the river boundary on places likely to have hyporheic exchange. In PMPATH, each of the locations was given their own colour to differentiate them. An arrow-mark was placed every 10 hours while the program traced the particle to the other side of the area. In Simulation B, 30 MODFLOW simulations were performed for 16 locations at the eastern side of the model. All starting locations for the particle experiments are shown in Figure 5. The residence times were compared to the average flow velocity of the Petit Buëch. The flow velocity was measured by injecting uranine dye tracer in the river and recording the time it takes to reach a measurement point.

After running the MODFLOW model, the hydraulic head was plotted and extracted from the Digital Elevation Model to indicate the depth of the groundwater. To visualize the flux of water flowing out of the river and into the river, observations were combined with calculations. Exchange volumetric flux between river and groundwater was calculated using

$$Q = \left(\frac{K_c \cdot L \cdot w}{h_c} \right) \cdot (h - h_{riv}) \quad (3)$$

where K_c is the hydraulic conductivity (m/s), L is the length and w is the width of the river within a cell (m), h_c is the thickness of the layer, h_{riv} is the hydraulic head of the river and h is the groundwater head (Brunner et al., 2010 and McDonald and Harbaugh, 1988). The Raster Calculator from ArcGIS was used for the calculation of these fluxes. The locations for Simulations A and B (Figure 5) were chosen before performing the above visualization of fluxes in and out of the river.

3. Results and Discussion

3.1 Morphological units

Morphological units were observed from aerial photographs and field observations. There are many vegetation differences noticeable in the area. Some areas do not have vegetation at all, while locations opposite to the river are covered by large bushes and small trees. In between those boundaries, first, second and third year vegetation can clearly be distinguished. Striking is that boundaries between vegetation types often coincide with changes in the landscape, i.e. small dunes and larger scale ripples.

Besides changes in vegetation, morphological units also were distinguished by differences in height. Cross sections A-A' and B-B' (Appendix A) were made to show that a gully is present at a distance of 20 to 25 meters from the river, followed by an increase of height of more than 1 meter. This was an argument to classify the area next to the river as different morphological unit from the higher lying area on the other side of the gully. It can also be noticed from the cross sections that there is a height difference between the bottom of the river and the gully. That causes small channels from the main river towards the gully during increased flow discharge. From these swales the former flow direction can be distracted using the imbrication of the gravel parts.

Using changes in vegetation and differences in height, the area was divided into six separate units. This is presented in Appendix B(IV). The outer unit along the river did not have any vegetation cover and the inner parts of the area are covered with small trees and bushes. Remarkable is that the shape of the morphological units is similar to the curve of the river.

The Petit Buëch is a whitewater river, meaning that in melting season the discharge of the river increases and large boulders are transported downstream. With an increasing discharge of the river, floodings occur and the course of the main channel of the river changes. Vegetation starts to grow on newly formed beds on the point bar after the course of the main channel changes. The separation and shape of the morphological units shown in Appendix B(IV) can be explained by this phenomenon. The outer course of the point bar has the least amount of vegetation (lightest green). Therefore this morphological unit was probably flooded during the latest melting season, thereby destroying any fresh vegetation.

From the morphological observations it can be extracted that the gully at 20 to 25 meters from the river (Appendix A) was the former main channel. During melting season the area outside of the gully might have been flooded causing the main channel to migrate outwards. The fact that larger boulders were found in the gullies and swales supports the above statement. The large boulders should have been transported by large river channels. The division between other morphological units can be supported by similar observations. Often at these boundaries similar gully structures can be seen.

By making DGPS measurements it was possible to create accurate digital elevation models using ArcGIS. DGPS measurements were interpolated using the Topo to Grid interpolation method in ArcGIS. The Digital Elevation Model (DEM) is

shown in Appendix B(III). Some DGPS measurement locations can be recognized as point elevations instead of lines equal in height. Especially at locations close to each other having a large difference in height (ridges) the point elevations are visible. This could have been prevented by performing more DGPS measurements, thereby creating a more accurate interpolation. Overall, the DEM which was created using this method was sufficient in scope of this study because the details necessary for this study (i.e. ridges and gullies) are visible. The separation of the area in different morphological units (Appendix B(IV)) can be supported using the DEM as well as the aerial photograph of the area (Appendix B(II)). Both the aerial photograph and the DEM show the exact locations of gullies. The gully seen in Appendix A can be distinguished, but also gullies and swales on the eastern side of the floodplain are visible.

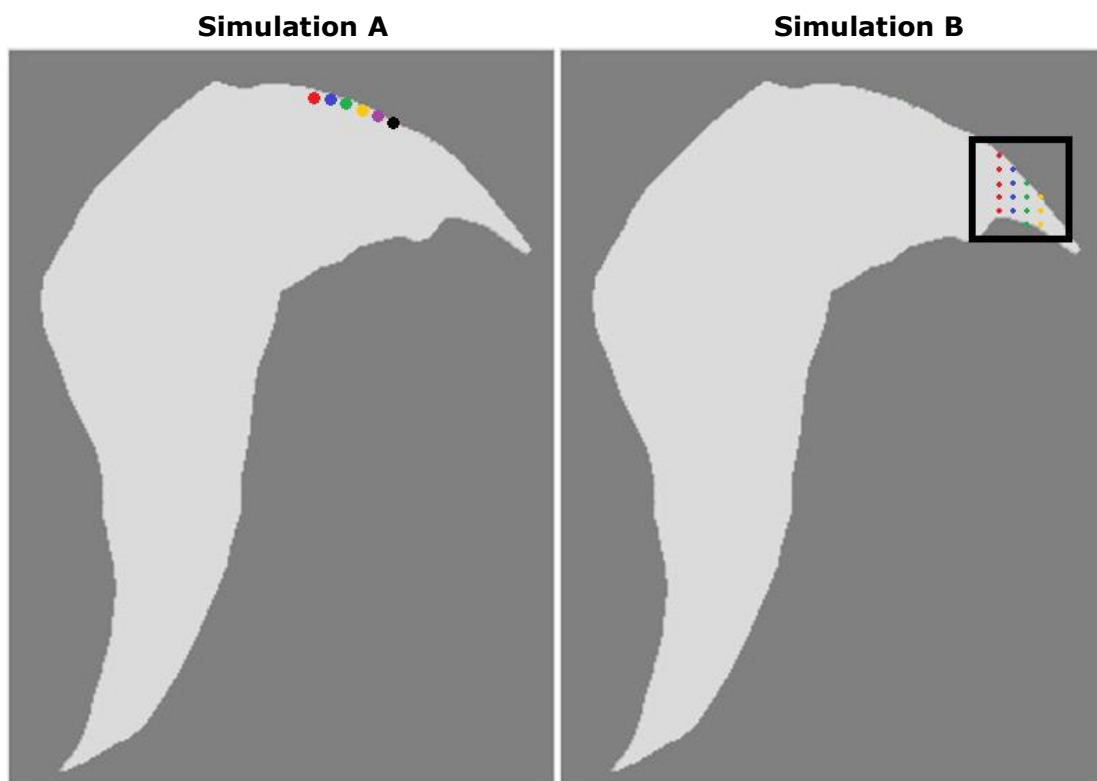


Figure 5 – Starting locations for the particle trace simulations in PMPATH (Simulation A: 50 generated fields on 6 locations, Simulation B: 30 generated fields on 16 locations).

3.2 Hydraulic Conductivity

The tracer experiments resulting in 39 breakthrough curves are shown in Appendix D. Two distinct curves are shown in Figure 6, Measurement-01 showing a smoother curve than Measurement-11. The former is the typical result of a tracer experiment, starting with a constant value, followed by a rapid increase and a gradual decrease towards its initial value. In such a curve, the difference between time until maximum EC (t_{\max} , red line) and time until 50% ($t_{50\%}$, green line) is rather small. In contrary, less smooth curves as shown in by measurement-11 have large differences between t_{\max} and $t_{50\%}$. The smoothest curves were observed on locations with visual hyporheic exchange, where water clearly exfiltrates the sediments.

In Figure 6 it can be seen that the $t_{50\%}$ is later than the t_{\max} . For the calculation of groundwater flow velocity, $t_{50\%}$ is chosen because of fast increasing and slowly decreasing curves like Measurement-11. In these cases, $t_{50\%}$ is a better representative for flow velocity, because a large percentage of tracer takes longer than t_{\max} to flow through the measurement point. Direct flow paths resulting in fast t_{\max} -values would underestimate the time for the bulk amount of tracer to reach the measurement point. Also, they do not take into account the tail of the curves, which is important for hyporheic exchange.

Some curves shown in Appendix D show variant shapes from the general shapes shown in Figure 6. Measurements 07 and 22 show two peaks, indicating multiple flow paths. All measurements were treated the same when calculating groundwater flow velocity.

Sieve experiments performed on 13 locations resulted in grain size distributions. In Figure 7 three example grain size distributions are shown; Appendix C shows all of them. Using Equation 2 described in the Methods Section, the porosity was calculated on the 13 locations. From Figure 7 it can be seen that steep curves represent large porosity (red and blue) and flat curves (green) represent small porosity. All resulting porosities are given in Table 2. It can be seen that the porosity varies between 0.18 and 0.34, which are typical values for a mixture of sand and gravel (Fetter, 1994). From all porosity measurements an interpolation was made using ArcGIS. The method which was chosen to interpolate the measurements was Topo to Grid. The resulting interpolation is given in Appendix B(V).

Formula 2 proved to be realistic for the calculation of porosity as all values were in range for mixed sand and gravel. Lower porosity values were found at areas having more sand and smaller particles in between the gravel and pebbles. Higher values were found at places with better sorted gravel and pebbles, for instance at the mouth of the gullies along measurements 01, 02 and 13.

Some remarks can be made regarding to the porosity interpolations. The porosity interpolation was based on 13 measurement locations, with most being in the middle of the area of research. Therefore, the interpolation is most reliable in the middle, whereas the interpolation at the southern and eastern locations is less reliable. For a larger reliability more measurements should be performed.

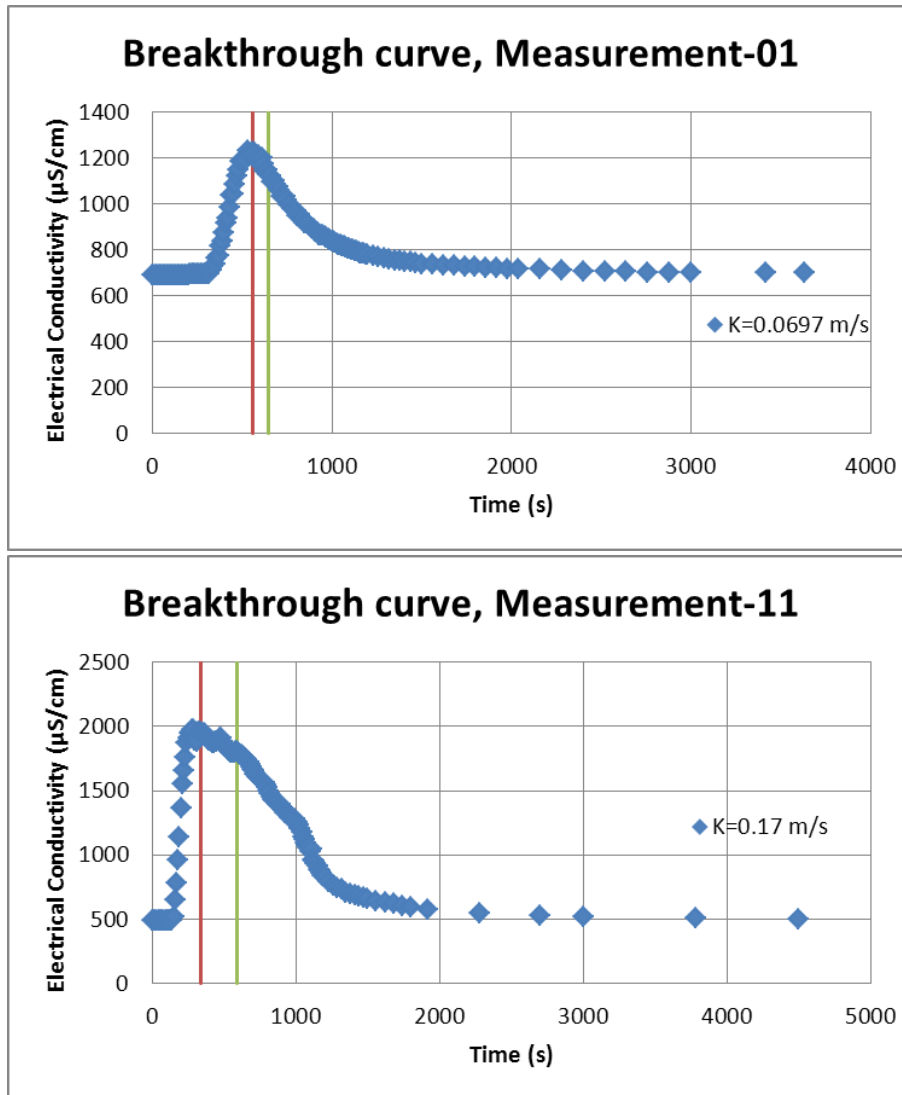


Figure 6 – Breakthrough curves for Measurements 01 and 11. Measurement 01 shows a smooth curve with small difference between peak time (red) and 50% value (green). Measurement 11 shows a steep curve with large difference between peak time (red) and 50% value (green).

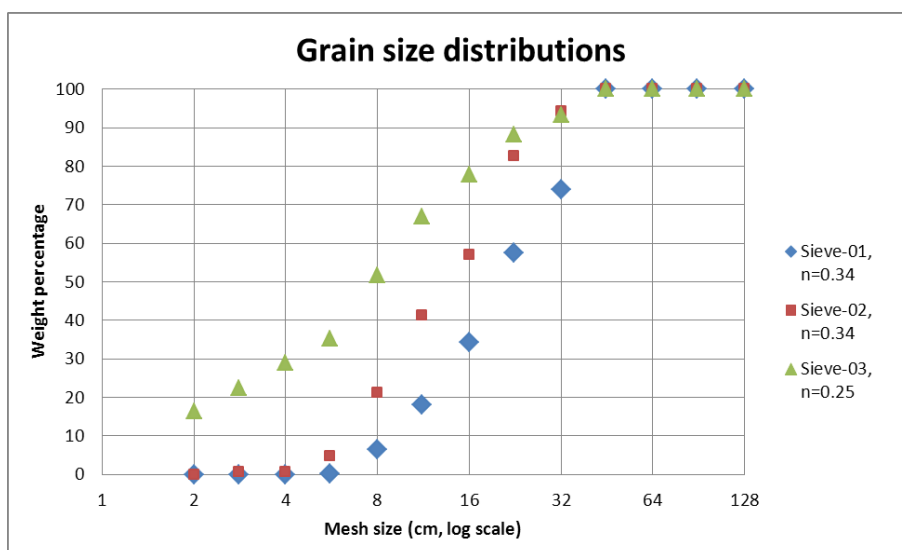


Figure 7 – Grain size distribution graphs for sieve experiments 01, 02 and 03.

Table 1 (left) – Hydraulic conductivity measurements.
Table 2 (right) – Porosity measurements.

<i>ID</i>	<i>Longitude</i>	<i>Latitude</i>	<i>K-value (m/s)</i>	<i>ID</i>	<i>Longitude</i>	<i>Latitude</i>	<i>Porosity</i>
measurement-01	718670.49	4926948.59	0.0697	Sieve-01	718655.40	4927019.00	0.34
measurement-02	718662.06	4926996.45	0.1782	Sieve-02	718657.22	4927035.74	0.34
measurement-03	718661.07	4927023.98	0.2651	Sieve-03	718654.46	4927046.77	0.25
measurement-04	718661.78	4927022.38	0.4626	Sieve-04	718653.57	4927073.43	0.31
measurement-05	718662.92	4926977.97	0.0162	Sieve-05	718665.84	4926992.66	0.24
measurement-06	718657.33	4927003.99	0.0332	Sieve-06	718683.41	4927062.20	0.21
measurement-07	718658.82	4927017.19	0.3693	Sieve-07	718696.22	4927083.76	0.18
measurement-08	718658.45	4926998.53	0.0040	Sieve-08	718674.79	4927105.28	0.25
measurement-09	718663.45	4926970.07	0.0141	Sieve-09	718692.64	4927119.23	0.23
measurement-10	718654.26	4927041.00	0.0403	Sieve-10	718726.12	4927023.60	0.28
measurement-11	718655.21	4927071.95	0.1700	Sieve-11	718737.00	4927058.00	0.23
measurement-12	718655.77	4927071.95	0.2400	Sieve-12	718711.09	4927044.22	0.24
measurement-13	718656.40	4927056.39	0.1103	Sieve-13	718711.91	4927019.79	0.32
measurement-14	718676.01	4927104.21	0.2404				
measurement-15	718672.87	4927105.17	0.0550				
measurement-16	718734.00	4927128.52	0.1524				
measurement-17	718656.70	4927012.90	0.4096				
measurement-18	718656.70	4927033.20	0.0274				
measurement-19	718655.19	4927049.02	0.1067				
measurement-20	718657.40	4927025.90	0.0626				
measurement-21	718659.15	4927045.42	0.1299				
measurement-22	718664.86	4927096.88	0.0102				
measurement-23	718657.95	4927060.69	0.0914				
measurement-24	718658.30	4927087.00	0.0101				
measurement-25	718664.90	4927098.20	0.0062				
measurement-26	718675.00	4927102.10	0.6382				
measurement-27	718675.00	4927102.20	0.4065				
measurement-28	718715.90	4927125.80	0.0441				
measurement-29	718720.60	4927128.70	0.0806				
measurement-30	718716.80	4927127.40	0.0083				
measurement-31	718727.20	4927126.30	0.1530				
measurement-32	718727.20	4927126.20	0.2034				
measurement-33	718730.40	4927130.10	0.2418				
measurement-34	718714.70	4927126.30	0.2969				
measurement-35	718724.90	4927129.40	0.0165				
measurement-36	718723.90	4927123.80	0.0454				
measurement-37	718742.10	4927125.90	0.0759				
measurement-38	718745.90	4927125.30	0.1282				
measurement-39	718745.30	4927123.90	0.0768				

All necessary parameters for calculating hydraulic conductivity with Darcy's Law were known after calculating the breakthrough curves (Appendix D) and interpolating the porosity (Appendix B(V)). The calculated values for hydraulic conductivity at all 39 locations are shown in Table 1. The values are also given in the breakthrough curves of Appendix D. The resulting hydraulic conductivities at the measurement locations varied from 0.004 m/s to 0.64 m/s. The calculations show an average hydraulic conductivity of 0.146 m/s, therefore representing an aquifer existing of well sorted gravel and pebbles according to Bear (1972). The interpolation of hydraulic conductivity values made using the Topo to Grid function of ArcGIS is shown in Appendix B(VI). For this interpolation all field measurements were used.

In Figure 8 the distribution of the 1000 points on which the analysis of variance is based is shown, together with the morphological units. Table 3 shows the results for the ANOVA performed on these data. For this statistical test the null hypothesis is that the average hydraulic conductivity for every area is equal. At a 95% confidence level, the null hypothesis can be rejected because the P-value is smaller than 0.05. However, Table 4 shows similarity in average and variance between some units and therefore student's T-tests were performed. The results (Table 5) show that there is no significant difference between units 1 and 4, units 1 and 5 and units 4 and 5 (at 95% confidence level). When comparing the interpolation with the vegetation units, it can be confirmed that units 1, 4 and 5 show a similar distribution of hydraulic conductivities (Figure 8). From this statistical analysis it can be concluded that the interpolated hydraulic conductivity is not dependent on the vegetation cover for all morphological units.

Table 3 – ANOVA, accepting the null hypothesis when $P\text{-value} > \alpha$ or $F < F_{crit}$.

Source of Variation	F	P-value	F crit
Between Groups	99.23	8.00E-71	2.38

Table 4 – Summary of the randomized locations in 5 units.

Units	Count	Sum	Average	Variance
1	385	372.74	0.968	0.968
2	185	116.08	0.627	0.627
3	148	103.21	0.697	0.697
4	151	147.57	0.977	0.977
5	106	100.77	0.951	0.951

Table 5 – Two-sample student's T-tests assuming unequal variances. The table shows the P-values for two-tail distributions, accepting the null hypothesis when $P\text{-value} > \alpha$ (green values).

	1	2	3	4	5
1	X	2.15E-56	2.15E-35	0.663	0.509
2		X	9.68E-05	8.51E-53	2.55E-27
3			X	1.18E-35	7.73E-19
4				X	0.309
5					X

The interpolated map of the hydraulic conductivity was exported as ASCII-file from which the average hydraulic conductivity of the interpolated values was calculated (0.129 m/s). The average value of the interpolated hydraulic conductivity is an average value for the entire grid and therefore gives a better estimation of the average hydraulic conductivity over the area than the average of the 39 data points (0.146 m/s).

Due to the method of interpolation, some locations within the research area resulted in negative values. To be in range of the measured hydraulic conductivity, all K-values less than 0.005 m/s were adjusted and replaced with 0.005 m/s. The average hydraulic conductivity of the resulting grid values is 0.129 m/s. Further on, this value will be referred to as K_{interp} . It should be noted that this is the average value for the entire grid, including inactive cells.

As the statistical analysis showed no correlation between hydraulic conductivity and vegetation cover, various conclusions can be drawn. Either the number of measurements used for the interpolation or the method used for the interpolation is not sufficient, as Morgan et al. (1998) shows that hydraulic conductivity is dependent on vegetation cover. All porosity measurements were performed in the middle of the area, while EC measurements could only be performed along gullies in the least vegetated morphological units. Reasons for the absence of inland measurements are the higher topography, which made it impossible to reach the groundwater level and to show hyporheic exchange.

Therefore the interpolation shown in Appendix B(VI) is accurate in the vicinity of the measurement points, but less accurate at further distances in more vegetated areas. The uncertainty of this area is large, as well as for the southern and eastern parts of the area. More measurements should have been performed to increase the certainty.

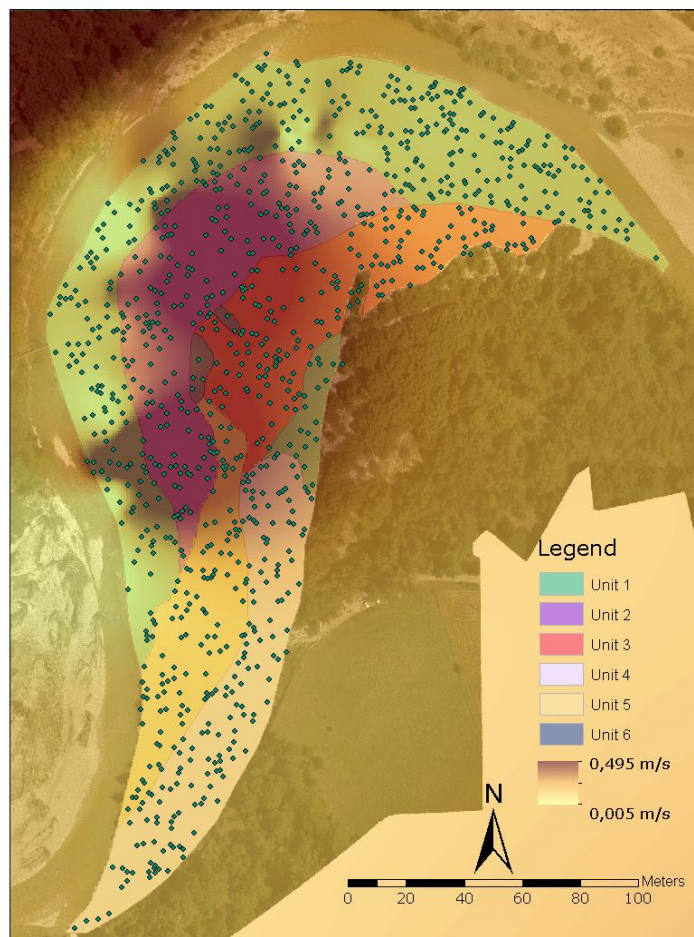


Figure 8 – Distribution of 1000 random points within the morphological units. Darker areas represent higher hydraulic conductivity values.

3.3 MODFLOW model

Model input

For the extension of the MODFLOW model, the 322 by 239 grid was divided in active cells and inactive cells. In Appendices F and G the results of the simulations are shown. In these results the inactive cells are visualized as gray cells, therefore leaving the area representing the point bar active. The northern and western boundaries of the active cells represent the constant head boundaries.

The influence of the thickness of layers of the model on the residence time is shown in Table 6 and Figure 9. It can be seen that the residence time of the particles is linearly dependent on the layer thickness. Each of the relations has a coefficient of determination larger than 0.95. Due to the linear relationship between residence time and the thickness of the layers, changing the thickness does not make a fundamental difference. To correspond with the cell size of the model, a layer thickness of 1 meter was chosen. The number of layers was set to 4, equal to the total change in elevation (see Appendix B(III)). The elevation of the top and bottom of layers was set in accordance to the number of layers and their thickness.

Because of the nature of the area (being a point bar in a meander of the river), the top layer was chosen to be unconfined (*type 1*). The lower layers were chosen to be "either confined or unconfined" (*type 3*), depending on their transmissivity calculated by the model.

To estimate residence time distributions of the research area, simulations A and B were performed using random hydraulic conductivities. In those simulations, ASCII-files based on the interpolated values for the porosity were used (Appendix B(V)).

Table 6 – Residence time (h) of particles in relation with the layer thickness (m).

Layer Thickness (m)	Particle number		
	1	2	3
0.5	190	210	270
1	190	210	280
1.5	200	220	300
2	205	225	310
2.5	210	230	320
5	250	280	355

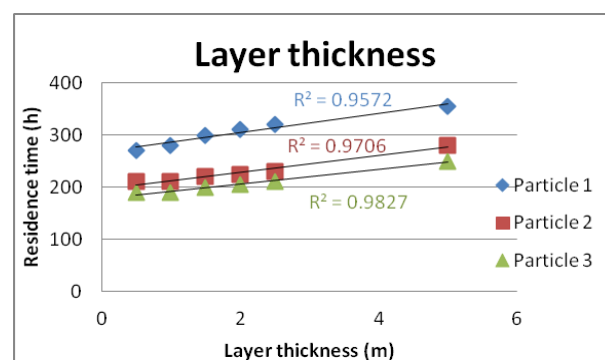


Figure 9 – Relationship between the layer thickness (m) and residence time (h) for three particles.

Field Generator and correlation length

The Field Generator needed the log value of the hydraulic conductivities which were used to calculate K_{interp} . Also the log value of the standard deviation was needed, resulting in respectively -0.96 for the average log value and 0.29 for the standard deviation of the log values. As can be seen in the resulting data input for the Field Generator (Figure 12), the correlation length had to be calculated.

Using correlation function of Excel it was not possible to distract the correlation length for distances equal to one meter (which is the cell size of the MODFLOW model) (Figure 10). The reason is that distances between measurement points are often larger than one meter, as can be seen in the insert. Therefore this method overestimates the correlation length. However, the large correlation for values below 3 meter show that there is a spatial correlation between the interpolated hydraulic conductivity values and therefore the Gstat method can be applied.

A semivariogram was made using the Gstat function of PCRaster. Different models can be used, of which the spherical model was chosen to model the correlation length. The spherical model gives a clear estimation of correlation length (Pebesma, 2001). For the semivariogram, a cutoff of 30 meters was chosen and a width of 3 meter. The resulting semivariogram gave a correlation length of ~ 13 meters reaching a semivariance of 0.38 (Figure 11). In the Field Generator, this results in ratios of ~ 0.04 and ~ 0.06 for the correlation length divided by the field width along rows and along columns. To summarize, all input data for the generation of 100 random fields are shown in Figure 12.

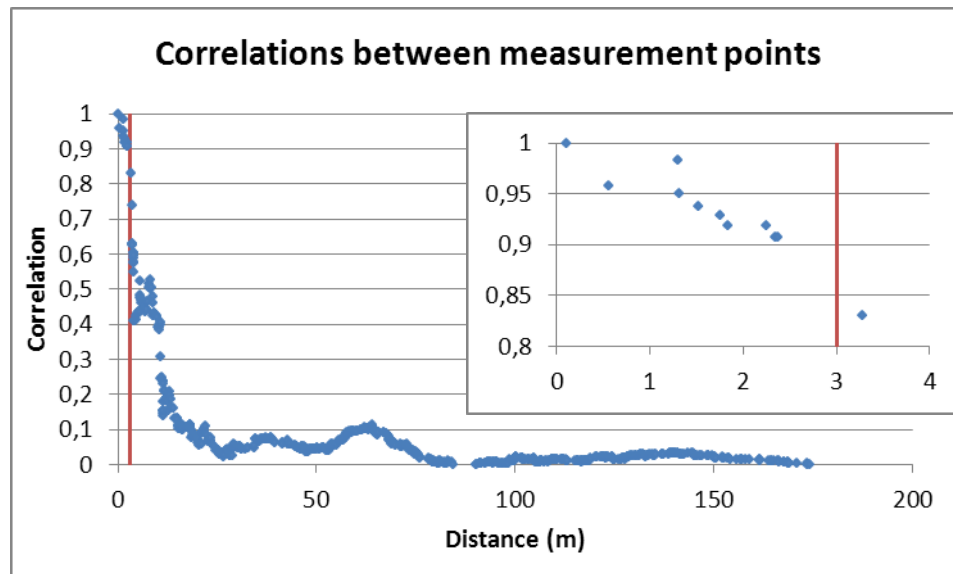


Figure 10 – Correlations between measurement points versus the distance between them. The red line represents the 3 meter value. The insert to the right shows a close-up for values up to 4 meters.

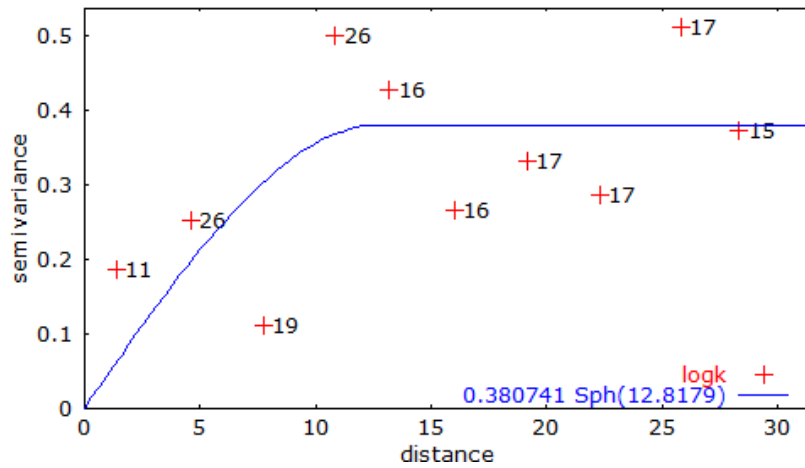


Figure 11 – Semivariogram for the relation between distance and hydraulic conductivity (Gstat).

Parameters	
Number of Realizations [1 to 999]:	<input type="text" value="100"/>
Mean Value (log10) [-30 to +30]:	<input type="text" value="-.96"/>
Standard Deviation (log10) [0 to 30]:	<input type="text" value=".29"/>
(Correlation Length/Field Width) along rows [0 to 1]:	<input type="text" value=".04"/>
(Correlation Length/Field Width) along columns [0 to 1]:	<input type="text" value=".06"/>
Number of Rows [2 to 500]:	<input type="text" value="322"/>
Number of Columns [2 to 500]:	<input type="text" value="239"/>

Figure 12 – Data input for the Field Generator.

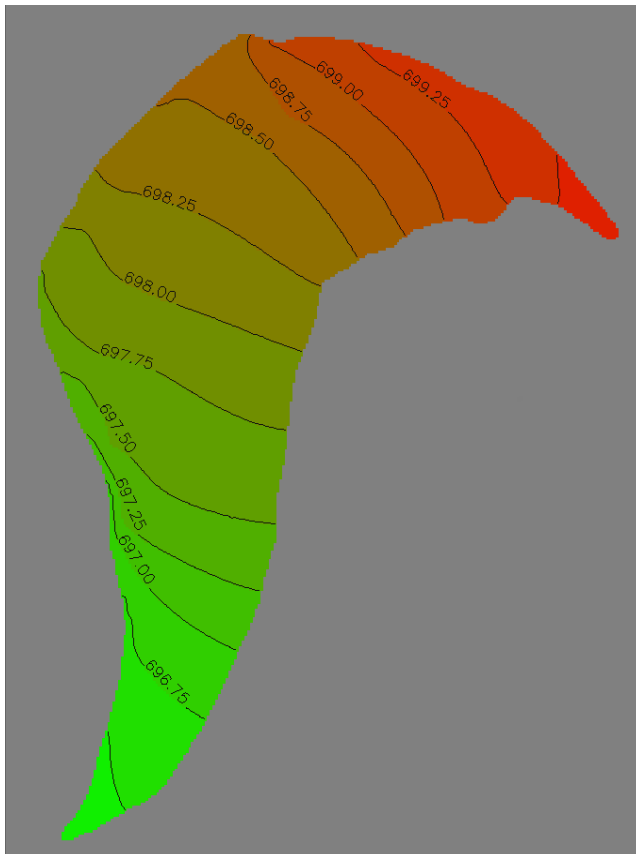


Figure 13 – Hydraulic head after running the MODFLOW model using interpolated hydraulic conductivity.

To verify the data generated using the Field Generator, the average hydraulic conductivity and standard deviation of ten randomly generated fields were compared to the input values. Average logarithmic values for the first ten randomly generated grids were roughly the same as the input values (-0.96 and 0.29). Therefore the generated grids were considered to be relevant for further usage. The correlations were also considered to be similar to the input values, because of the reliability of the Field Generator with regard to the average value and standard deviation. One remark is that the only a small part of the entire grid is active. That may cause generated grids to have a larger difference with the interpolated grid. To minimize the effect of large differences between randomly generated grids, the PMPATH simulations were performed on multiple MODFLOW simulations.

Infiltration and exfiltration fluxes

Using all input values for the MODFLOW simulations, it was possible to create maps showing the hydraulic head differences within the study area. Figure 13 shows the hydraulic head generated by MODFLOW after running the model. It can be seen that there is a gradient in the southern direction, as was expected from the flow directions of the river and the gullies. In Figure 14, the hydraulic head was extracted from the Digital Elevation Model (Appendix B(III)) to show the depth of the groundwater below ground surface. The map is the most representative map of the fieldwork area, considering that it shows locations where groundwater reaches the surface. Blue areas having a negative depth indicate surface flow.

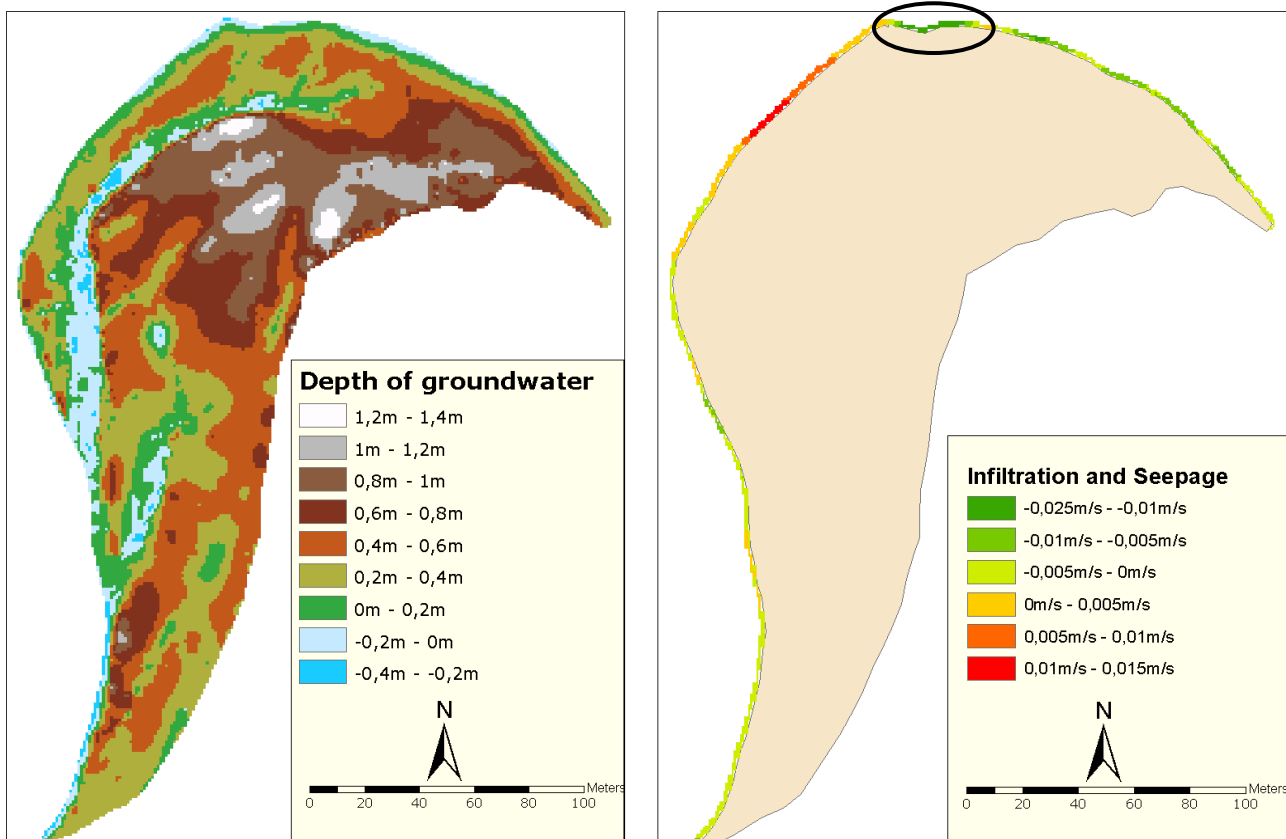


Figure 14 (left) – Depth of groundwater, negative values indicate surface flow.

Figure 15 (right) – Amount of infiltration and seepage, negative values indicate infiltration.

Equation 3 was used for the calculation of infiltration and seepage fluxes along the boundary between the river and the mainland. It should be noted that Brunner et al. (2010) analyzed MODFLOW for estimating fluxes using this equation. He concluded that MODFLOW underestimates infiltration fluxes.

In Equation 3, the length of the river within a cell, the width of the river and the layer thickness were assumed to be equal to the cell size (i.e. 1m). The resulting fluxes are shown in Figure 15. They indicate major infiltration at the upstream side of the area (green, indicated by negative values) and major seepage at the western side (red, indicated by positive values). The downstream side shows alternating locations of minor infiltration and seepage.

The location with the largest infiltration, indicated by the circle in Figure 15, corresponds to observations in the field and the results of Figure 14. Observations show that at that location, the river becomes broader and more shallow, while downstream the river narrows and becomes deeper (see the aerial photograph in Appendix B(II) and Figure 17). NE-SW oriented swales are present at this location.

The sum of all fluxes should be equal to zero in order to be in steady state. However, the result of Figure 15 shows that there is a surplus of 1.6 m/s of infiltration. In the calculation of fluxes, the exfiltration of water into gullies is not included. An explanation for the surplus may be exfiltration of water into surface waters on the point bar such as gullies. Figure 17 (red arrows) shows the possible infiltration of groundwater in the direction of the largest gully (mentioned in Section 4.1). The water can exfiltrate into the gully, which eventually debouches into the river, thereby nullifying the surplus of infiltration.

Figure 16 shows PMPATH traces of particles released in the northern infiltration area. The traces show particles flowing through the mainland similar to the direction of the gully shown in Figure 17. Exfiltration in the northwestern part of the area is an indication of groundwater flowing directly from the infiltration point to the exfiltration point, without flowing through the study area.

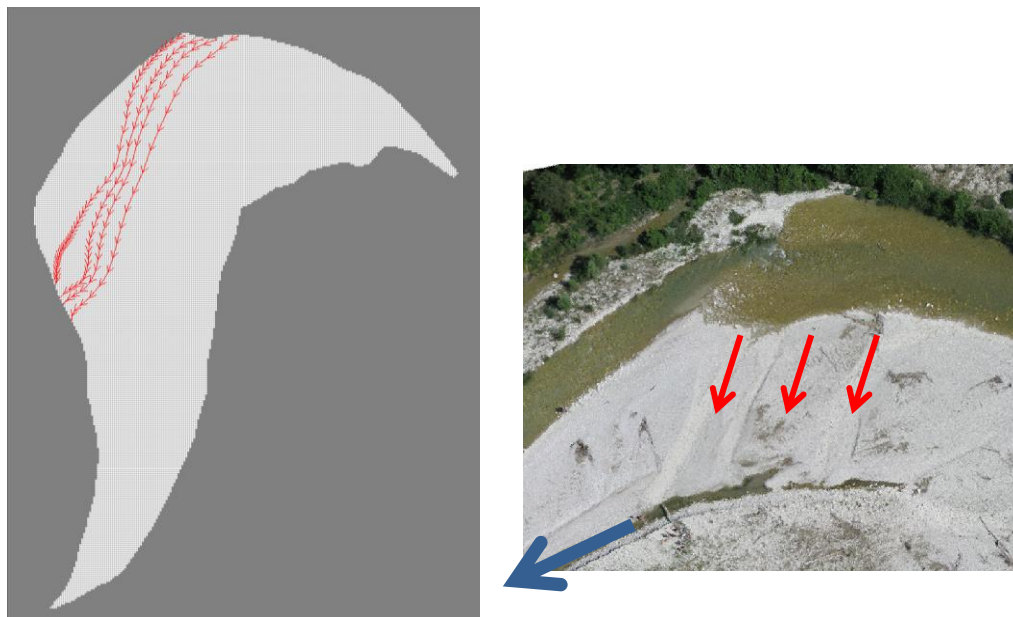


Figure 16 (left) – PMPATH traces of particles released at the location of largest infiltration.

Figure 17 (right) – Location of infiltration. Red Arrows indicate infiltration, blue arrow indicates surface flow.

Simulation A

Flow paths of particles across the study area were visualized using the particle tracing program PMPATH. The starting locations for Simulations A and B are shown in Figure 5 (respectively A and B). Appendix B(I) gives an overview of the flow paths from the interpolated average hydraulic conductivity data (K_{interp}) combined with an aerial photograph of the research area. It can be seen that water infiltrating from the river flows through the research area to the other side. All runs show exfiltration from the sediments into the river in the same area as observed in the field.

In Appendix E(I) six PMPATH runs for Simulation A are given. The runs can be compared to the runs of K_{interp} and K_{average} . While K_{interp} uses the interpolated values from the 39 measurement points, K_{average} fills the entire grid with the average hydraulic conductivity. The course of the flow paths is compared in Appendix E(II) and Figure 18, showing five runs from each particle in one plot. All runs show exfiltration in the location just south of the mouth of the largest gully (Section 4.1). It can be seen that there is some variation between the runs. Runs 2 and 3 show flow paths close to each other, while in runs 4 and 6 they lay further apart (Appendix E(I)).

The runs show a general trend of being roughly the same until ~ 150 hours, after which the runs begin to differentiate. The trend until ~ 150 hours is most influenced by the fact that all runs have the same starting location. After longer residence times, the chance for particles to reach locations with different porosity or hydraulic head enlarges. Reaching a different porosity or elevation influences the flow path. This can also be noticed in Figure 18, where one model run shows more westerly oriented flow direction than the other runs. Residence times were determined by the number of arrow-marks on the flow paths, each arrow mark being 10 hours.

Appendix F shows the residence of the modelruns for Simulation A. Also the frequency table and the residence time distributions (RTD's) are shown. Some residence times are missing from the A6 particle simulation. These were runs showing seepage by returning to the river instead of flowing through the study area. The seepage particles were left out of the residence time distributions as they were not comparable to the other particles. Residence time increases when going from the west to the east (i.e. upstream). This is the result of an increasing distance to the other side of the point bar with the most eastern particle (A6, black) having the largest distance to cover. The average residence time for all particles is 480 hours. Water infiltrating the point bar takes 20 days to exfiltrate into the river again. Uranine experiments in the Petit Buëch showed that it took ~ 20 minutes for the tracer to reach a location ~ 600 meter downstream. That results in an average flow velocity of 0.5 m/s. It would take 8 to 9 minutes to reach the location of exfiltration using the location of infiltration in Figure 18. Hyporheic exchange causes a retardation of a factor of 1000, assuming exfiltration only takes place into the river.

The RTD's for simulations of particles A1 (red), A2 (blue) and A3 (green) show similarities in peak times. Each of them have peak values at 400 to 500 hours and average residence times of 400 to 430 hours. RTD's for particles A4 (orange), A5 (purple) and A6 (black) show increasing peak and average residence times, up till an average residence time of 615 hours for A6.

The flow paths (Appendix E(I)) and the residence times (Appendix F) of the simulations were compared to the modelruns for K_{interp} and $K_{average}$. The flow paths show similar flow direction, however the simulations are less smooth and some show larger variation between the particles. The residence times have increased by 40 to 50% when using randomly generated hydraulic conductivities. This might be the result of generating entire fields of 322 by 239 cells while only the active cells were needed. Another point of discussion is the water exfiltrating into the gully, decreasing the residence time. Exfiltration to the gully is not taken into account during these simulations.



Figure 18 – Five modelruns for particle A1 (Simulation A).

Simulation B

Simulation B was performed on 16 locations at the eastern side of the model, each having a separate colour (Figure 5). Appendix G shows the flow paths for K_{interp} , $K_{average}$ and the first 10 runs. The residence times are shown in Appendix H. Because all locations of infiltration were chosen in close proximity, one frequency table (Table 7) leading to one RTD (Figure 19) was made. Similar to Simulation A, some runs in Simulation B showed seepage and were removed from the RTD.

Table 7 – Frequency table for the residence times of Simulation B.

RT (h)	Freq.
0	0
100	0
200	0
300	0
400	34
500	114
600	91
700	101
800	62
900	28
1000	17
1100	10
1200	7
1300	4
1400	3
1500	2
1600	3
1700	1

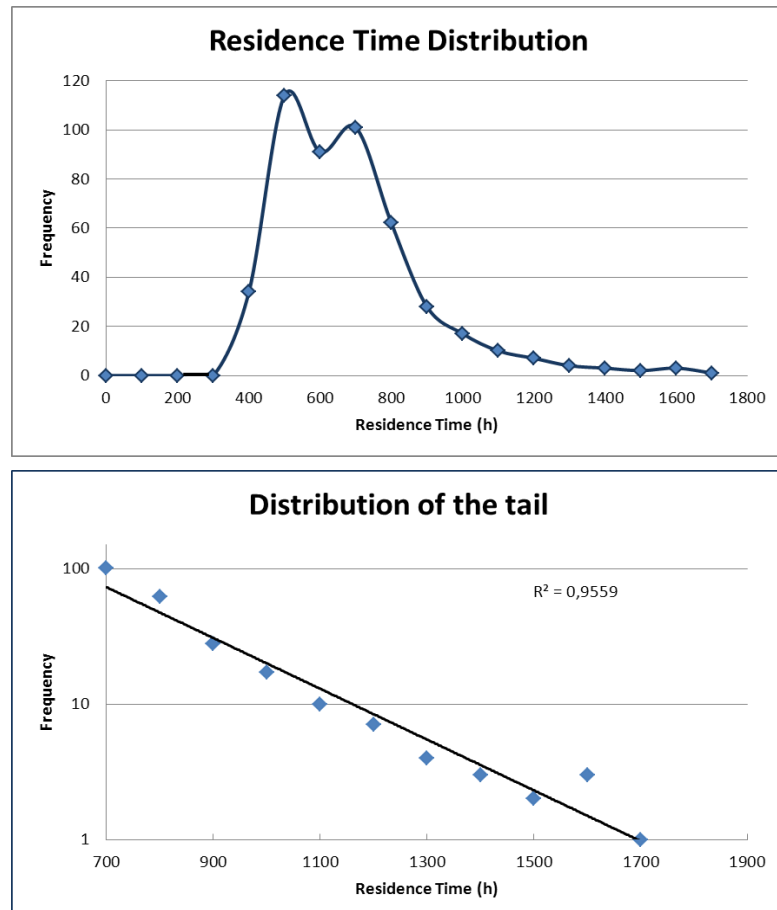


Figure 19 – Upper graph: Residence Time Distribution of simulation B. Lower graph: distribution of the tail of the RTD on a semi-log scale.

The distribution of flow paths of the runs in Appendix G is similar to the runs of K_{interp} and $K_{average}$ with all particles showing roughly the same flow path. This can be explained by the small size of the area of infiltration and the course along the outer boundary all flow paths have to follow.

Residence times are longer than the residence times from Simulation A. This is equal to the trend noticed in Simulation A, with longer residence times for the most eastern infiltration points. Particles C6 (yellow) and D6 (green) show residence times of over 1000 hours.

The frequency table of Table 7 and the RTD of Figure 19 (upper graph) show peak exfiltration at 500 to 700 hours. The peak is followed by a long tail, reaching residence times of over 1600 hours. Figure 19 (lower graph) shows the distribution of the tail plotted on a semilog scale. The exponential trendline has a coefficient of determination of 0.956, proving an exponential distribution.

Generally, the shape of the RTD's and the average residence times of Simulations A and B are similar. Difference in mean residence times can be explained by distance covered by the flow paths (i.e. larger distance results in larger mean).

In light of the goals of this research it was possible to perform MODFLOW and PMPATH simulations of hyporheic exchange, shown in Simulation A and Simulation B. According to the map of the infiltration and exfiltration fluxes (Figure 15), the starting locations for the simulations were chosen on locations with infiltration. Together with the field observations of hyporheic exchange, it can be stated that the simulations are representable for the study area.

3.4 Recommendations

Some general points of discussion for the methods leading to the results have been mentioned before. For further research, these methods could be adjusted and improved. These include the methods for interpolation of the measurements used in ArcGIS. More field measurements would result in more accurate interpolations.

Furthermore, the usage of the Field Generator could be improved. The Field Generator generated data for the entire grid of 322 by 239 cells instead of the active cells only. The latter would result in grids more comparable to the original interpolation.

Last point of improvement could be the usage of boundaries in MODFLOW. In this study, the northern boundary was set as constant head boundary, while the southern boundary was specified as transition from active to inactive cells. In the study area, a transition of vegetation was noticed on the southern boundary. However, groundwater continues to flow through this area. Therefore it would be more representative if this boundary showed a gradual decrease of hydraulic conductivity, eventually stopping groundwater flow.

4. Conclusions

Hydrological research was performed on a point bar of the river Petit Buëch in Southern France. Tracer experiments were conducted in order to calculate the hydraulic conductivity on multiple locations. The number of tracer experiments proved to be sufficient to make interpolations, but performing more experiments increases the reliability of the results. Also porosity measurements and DGPS measurements were conducted. Interpolations for porosity, elevation and hydraulic conductivity were made using ArcGIS. The porosity measurements and interpolations gave values between 0.20 and 0.35, indicating a mixture of sand and gravel. The interpolations for the hydraulic conductivity gave values between 0.005 m/s and 0.5 m/s. That indicates the presence of locations with low conductivity, as shown in Figure 2.

All interpolations were imported into hydrological modelling program MODFLOW. A hydrological model was made and randomly generated grids of hydraulic conductivity were used to run the model. These model runs resembled the original run using the interpolated hydraulic conductivity. Particles were added in to the model using PMPATH and residence times were measured using the MODFLOW runs with randomized hydraulic conductivity fields. Residence time distributions show that it takes particles an average time of 20 days to transport through the point bar of the river. The tails of the RTD's show an exponential distribution.

The calculation of fluxes in the study area indicates a 1.6 m/s surplus of water infiltrating the point bar, maybe even more due to underestimation of the MODFLOW model (Brunner et al., 2010). It can be concluded that either water exfiltrates at locations beyond the study area, or water exfiltrates in gullies which debouch into the river.

The results of this study can be extrapolated to comparable and larger regions. These regions should satisfy conditions like being a point bar on a whitewater river. Differences in hydrology and morphology should be taken into account by using site-specific DGPS, porosity and hydraulic conductivity measurements. Infiltration and exfiltration should be carefully measured, especially when gullies are present.

It can be concluded that it is possible to master the process of hyporheic exchange using ArcGIS, MODFLOW and PMPATH. Hyporheic exchange causes surface water to infiltrate into the sediments of the point bar and will be retarded depending on the location of infiltration. Infiltration at large distance from the meander bend will take longer to reach the exfiltration point at the downstream side of the point bar.

5. Acknowledgements

During this study I have learned almost as much as during my entire time as a student. Not only did I learn a lot of the theoretical and practical matters of the subject, but also about my distribution of time and setting priorities. The latter did not always go as well as I would have liked, although I am proud of the result. I could not have achieved this result without the patience, support and guidance of Dr. Marcel van der Perk. I would express my gratitude for never stopping to believe in a good result. Performing research in the field, making models on the computer and finishing this thesis would not have been possible without him.

Furthermore, I would like to thank all people who helped me during my fieldwork. These were the students performing experiments and teachers accompanying them. Experiments performed by the students were revisited and some made it into this thesis. Also thanks to Maarten Zeylmans van Emmichoven for letting me use the GISlab and helping me to use MODFLOW on the computers.

Then there were my friends who provided me with fresh insights regarding the subject. While they were finishing their studies, they motivated me to finish mine. Their progress stimulated me to get back to work on my thesis.

At last but not least I would like to thank my little brother and my parents. They kept on supporting me during the entire process. Even on moments that my mind was not focussed on this thesis at all, they kept pushing me to continue which lead to this result.

6. References

- Battin, T. J., Kaplan L. A., Newbold, J. D. and Hendricks, S. P. (2003). A mixing model analysis of stream solute dynamics and the contribution of a hyporheic zone to ecosystem function, *Freshwater Biology* 48: 995-1014.
- Bear, J. (1972). Dynamics in Fluids in Porous Media, Dover Publications.
- Beard, D.C. and Weyl, P.K. (1973). Influence of texture on porosity and permeability of unconsolidated sand, *AAPG Bulletin* 57: 349-369
- Boano, F., Packman, A. I., Cortis, A., Revelli, R. and Ridolfi, L. (2007). A continuous time random walk approach to the stream transport of solutes, *Water Resources Research* 43: W10425.
- Boano, F., Revelli, R. and Ridolfi, L. (2007). Bedform-induced hyporheic exchange with unsteady flows, *Advances in Water Resources* 30: 148-156.
- Boulton, A. J., Findlay, S., Marmonier, P., Stanley, E. H. and Valett, H. M. (1998). The functional significance of the hyporheic zone in streams and rivers, *Annual Reviews of Ecological Systems* 29: 59-81.
- Bouwer H. and Rice, R. C. (1976). A slug test for determining hydraulic conductivity of unconfined aquifers with completely or partially penetrating wells, *Water Resources Research* 12-3: 423-428.
- Brunner P., Simmons, C.T., Cook, P.G. and Therrien, R. (2010). Modeling surface water-groundwater interaction with MODFLOW: some considerations, *Groundwater* 48-2: 174-180.
- Cardenas, M. B., Wilson, J. L. and Zlotnik, V. A. (2004). Impact of heterogeneity, bed forms, and stream curvature on subschannel hyporheic exchange, *Water Resources Research* 40: W08307.
- Cardenas, M. B. (2009). A model for lateral hyporheic flow based on valley slope and channel sinuosity, *Water Resources Research* 45: W01501.
- Cey, E. E., Rudolph, D. L., Parkin, G. W. and Aravena, R. (1998). Quantifying groundwater discharge to a small perennial stream in southern Ontario, Canada, *Journal of Hydrology* 210: 21-37.
- Chiang, W-H. and Kinzelbach, W. (1998). Processing MODFLOW, a simulation system for modeling groundwater flow and pollution. Springer
- Chiang, W-H. (2005). 3D-Groundwater modelling with PMWIN, Second Edition. A simulation system for modelling groundwater flow and transport processes. Springer
- Choi, J., Harvey, J. W., and Conklin, M. H. (2000). Characterizing multiple timescales of stream and storage zone interaction that affect solute fate and transport in streams, *Water Resources Research* 36(6): 1511-1518.
- De Smedt., F. (2007). Analytical solution and analysis of solute transport in rivers affected by diffusive transfer in the hyporheic zone, *Journal of Hydrology* 339: 29-38.
- Dent, C. L. and Henry, J. C. (1999). Modeling nutrient-periphyton dynamics in streams with surface-subsurface exchange, *Ecological Modeling* 122: 97-116.
- Dingman, S. L. (2002). Physical Hydrology, 2nd edn, Prentice Hall, New Jersey.
- ESRI 2011. ArcGIS Desktop: Release 10. Redlands, CA: Environmental Systems Research Institute.
- Fetter, C.W. (1994). Applied Hydrogeology, 3rd edition. Upper Saddle River, NJ: Prentice Hall, Inc.
- Freeze, R. A. and Cherry, J. A. (1979). Groundwater, Prentice Hall, New Jersey.

Frings, R. M., Kleinhans, M.G. and Vollmer, S. (2008). Discriminating between pore-filling load and bed-structure load: a new porosity-based method, exemplified for the river Rhine, *Sedimentology* 55: 1571-1593

Frings, R. M., Schüttrumpf, H. and Vollmer, S. (2011). Verification of porosity predictors for fluvial sand-gravel deposits, *Water Resources Research* 47: W07525.

Ge, Y., Boufadel, M. C. (2006). Solute transport in multiple-reach experiments: Evaluation of parameters and reliability of prediction, *Journal of Hydrology* 323: 106-119.

Gleick, P. H. (1996). Water resources, *Encyclopedia of Climate and Weather*, ed. by S. H. Schneider, Oxford University Press, New York, 2: 817-823.

Gooseff, M. N., Wondzell, S. M., Haggerty, R. and Anderson, J. (2003). Comparing transient storage modeling and residence time distribution (RTD) analysis in geomorphically varied reaches in the Lookout Creek basin, Oregon, USA, *Advances in Water Resources* 26: 925-937.

Harvey, J. W. and Bencala, K. E. (1993). The effect of streambed topography on surface-subsurface water exchange in mountain catchments, *Water Resources Research* 29(1): 89-98.

Haggerty R., Wondzell, S. M. and Johnson, M. A. (2002). Power-law residence time distribution in the hyporheic zone of a 2nd-order mountain stream, *Geophysical Research Letters* 29(13).

Hutchinson, M. F. (1988). Calculation of hydrologically sound digital elevation models. Paper presented at Third International Symposium on Spatial Data Handling at Sydney, Australia.

Hutchinson, M. F. (1989). A new procedure for gridding elevation and stream line data with automatic removal of spurious pits, *Journal of Hydrology* 106: 211-232.

Janzen, K. (2008). Hyporheic flow in a mountainous riverine system, a thesis, Department of Geography, University of Saskatchewan, Saskatoon.

Lautz, L. K. and Siegel, D. I. (2006). Modeling surface and ground water mixing in the hyporheic zone using MODFLOW and MT3D, *Advances in Water Resources* 29.

Lautz, L. K., Siegel, D. I. and Bauer, R. L. (2006). Impact of debris dams on hyporheic interaction along a semi-arid stream, *Hydrological Processes* 20: 183-196.

MacDonald, M.G., and Harbaugh, A.W. (1988). A modular, three-dimensional finite-difference ground-water flow model. Reston, Virginia: USGS.

Marion, A., Zaramella, M. and Bottacin-Busolin, A. (2008). Solute transport in rivers with multiple storage zones: The STIR model, *Water Resources Research* 44: W10406.

Merkx, O.K. (2011). Electrokinetically induced removal of heavy metal from an aged, contaminated sludge – a laboratory experiment (MSc thesis), Universiteit Utrecht.

Morgan, R.P.C., Quinton, J.N., Smith, R.E., Govers, G., Poesen, J.W.A., Auerswald, K., Chisci, G., Torri, D. and Styczen M.E. (1998). The European Soil Erosion Model (EUROSEM): A dynamic approach for predicting sediment transport from fields and small catchments, *Earth Surface Processes and Landforms* 23: 527-544.

Mutz, M. and Rohde, A. (2003). Processes of surface-subsurface water exchange in a low energy sand-bed stream, *International Review of Hydrobiology* 88(3-4): 290-303.

Packman, A. I., Selehin, M. and Zaramella, M. (2004). Hyporheic exchange with gravel beds: basic hydrodynamic interactions and bedform-induced advective flows, *Journal of Hydraulic Engineering* 130(7): 647-656.

Pebesma, E. J. (2001). Gstat user's manual, Department of Physical Geography, Utrecht University.

- Polluck, D. W., (1994). User's guide for Modpath/MODPATH-PLOT, version 3: A particle tracking post-processing package for MODFLOW, the U. S. Geological Survey finite-difference groundwater flow model, *U. S. Geological Survey Open-File Report* 94-464.
- Rayne, T. W., Bradbury, K. R. and Mickelson, D. M. (1996). Variability of hydraulic conductivity in uniform sandy till, Dane County, Wisconsin, *Wisconsin Geological and Natural History Survey, Information Circular* 74
- Ryan, R. J. and Boufadel, M. C. (2007). Lateral and longitudinal variation of hyporheic exchange in a piedmont stream pool, *Environmental Scientific Technology* 41: 4221-4226.
- Schmidt, C., Bayer-Raich, M. and Schirmer, M. (2006). Characterization of spatial heterogeneity of groundwater-stream water interactions using multiple depth streambed temperature measurements at the reach scale, *Hydrology and Earth Sciences Technology* 10: 849-859.
- Simcore Software (2011), Processing MODFLOW, an integrated modeling environment for the simulation of groundwater flow, transport and reactive processes.
- Stofleth, J. M., Shields Jr., F. D. and Fox, G. A. (2007). Hyporheic and total transient storage in small, sand-bed streams, *Hydrological Processes* 22(12)
- Stonedahl, S. H., Harvey, J. W., Wörman, A., Salehin, M. and Packman, A. I. (2010). A multiscale model for integrating hyporheic exchange from ripples to meanders, *Water Resources Research* 46: W12539.
- Storey, R. G., Howard, K. W. F. and Williams, D. D. (2003). Factors controlling riffle-scale hyporheic exchange flows and their seasonal changes in a gaining stream: A three-dimensional groundwater model, *Water Resources Research* 39(2): 1034.
- Tonina, D. and Buffington, J. M., (2009). Hyporheic exchange in mountain rivers I: Mechanics and environmental effects, *Geography Compass* 3/3: 1063-1086.
- Triska, F. J., Duff, J. H. and Avanzino, R. J. (1993b). The role of water exchange between a stream channel and its hyporheic zone in nitrogen cycling at the terrestrial- aquatic interface, *Hydrobiologia* 251: 167-184.
- Wondzell, S. M. and Swanson, F. J. (1996b). Seasonal and storm dynamics of the hyporheic zone of a 4th-order mountain stream. II: Nitrogen cycling, *Journal of the North American Benthological Society* 15: 20-34.
- Wondzell, S. M., LaNier, J. and Haggerty, R. (2009). Evaluation of alternative groundwater flow models for simulating hyporheic exchange in a small mountain stream, *Journal of Hydrology* 364: 142-151.
- Wörman, A., Packman, A. I., Johansson, H. and Jonsson, K. (2002). Effect of flow-induced exchange in hyporheic zones on longitudinal transport of solutes in streams and rivers, *Water Resources Research* 38(1): 1-15
- Wörman, A., Packman, A. I., Marklund, L., Harvey, J. W. and Stone, S. H. (2007). Fractal topography and subsurface water flows from fluvial bedforms to the continental shield, *Geophysical Research Letters* 34.